Indonesian Journal of Science & Technology

Journal homepage: http://ejournal.upi.edu/index.php/ijost/

Bifunctional $CaCO_3$/HY Catalyst in the Simultaneous Cracking-Deoxygenation of Palm Oil to Diesel-Range Hydrocarbons

Rosyad Adrian Febriansyar[1], Teguh Riyanto[1,2], I. Istadi[1,2], Didi D. Anggoro[1], Bunjerd Jongsomjit[3]*

[1]Department of Chemical Engineering, Faculty of Engineering, Universitas Diponegoro, Semarang 50275, Indonesia.

[2]Laboratory of Plasma-Catalysis (R3.5), Center of Research and Services - Diponegoro University (CORES-DU), Integrated Laboratory, Universitas Diponegoro, Semarang, Central Java 50275, Indonesia.

[3]Department of Chemical Engineering, Faculty of Engineering, Chulalongkorn University, Bangkok 10330, Thailand.

*Correspondence: E-mail: istadi@che.undip.ac.id

ABSTRACT

Palm oil is a promising raw material for biofuel production using the simultaneous catalytic mechanism of the bifunctional cracking-deoxygenation reactions. Through the cracking-deoxygenation process, the chains of palmitic acid and oleic acid in the palm oil were converted to diesel-range hydrocarbons. The combination effects of CaCO3 and HY zeolite enhanced the bifunctional catalytic cracking-deoxygenation of palm oil into biofuel, because of the increasing acid and basic sites in the catalysts due to the synergistic roles of CaCO3 and HY. The introduction of CaCO3 on HY zeolite generated both a strong acid and strong basic sites simultaneously on the designed catalyst, which supports the bifunctional mechanisms of hybrid cracking-deoxygenation, respectively. The CaCO3 impregnated on the HY catalyst has a synergistic and bifunctional effect on the catalyst supporting cracking-deoxygenation reaction mechanisms as mentioned previously. The deoxygenation reaction required the bifunctional strong acid and strong basic sites on the CaCO3/HY catalyst through decarboxylation, decarbonylation, and hydrodeoxygenation reaction mechanisms. Meanwhile, the cracking reaction pathway was supported by the strong acid sites generated on the CaCO3/HY catalyst. In other words, the high acidity strength promotes diesel selectivity, whereas the high strength of basicity leads to the deoxygenation reaction.

ARTICLE INFO

Article History:
Submitted/Received 18 Nov 2022
First Revised 19 Dec 2022
Accepted 03 Feb 2023
First Available Online 07 Feb 2023
Publication Date 01 Sep 2023

Keyword:
Bifunctional,
Biofuel,
Calcium carbonate,
Cracking,
Deoxygenation,
Palm oil.

1. INTRODUCTION

Globally, the consumption of fossil fuel-based energy is predicted to grow, resulting in increased environmental pollution and limited fossil fuel supplies. About 80% of global energy consumption comes from fossil fuels (Hancsók *et al*., 2007). The use of renewable fuels is one of the essential aspects of reducing carbon dioxide emissions. Therefore, renewable fuels have the potential to be suitable replacements for fossil fuels. Vegetable oils-derived renewable fuels have recently attracted the attention of researchers seeking solutions to the difficulties provided by decreasing oil reserves, oil supply issues, and the growing usage of non-renewable fuels. Palm oil is a vegetable oil that is often utilized as a raw material in the production of biofuels due to its high long-chain hydrocarbon content, relatively equal saturated and unsaturated oil content, widespread availability around the world, and abundant availability particularly in Indonesia (Istadi *et al*., 2020a; Xu *et al*., 2017).

Palm oil is mainly composed of triglyceride containing three fatty acid chains, which are connected by a carboxyl group to glycerol, with a molecular structure that is like hydrocarbon (Seifi & Sadrameli, 2016). Additionally, it may be utilized to produce biofuels through catalytic cracking processes. Thermal and catalytic cracking can be used to produce biofuels (Xu *et al*., 2017; Zhao *et al*., 2018; Istadi *et al*., 2020b). The catalytic cracking process of palm oil is driven by a chain reaction mechanism that includes initiation, propagation, and termination, which is a simple and effective method for biofuel production from palm oil (Corma & Orchilles, 2000; Riyanto *et al*., 2020; Yigezu & Muthukumar, 2014). Kwon *et al.* (2011) reported that removing the oxygen content of used palm oil is required to improve biofuel quality by increasing energy density, decreasing viscosity, and stabilizing biofuels. However, the high amount of oxygen in palm oil cannot be used directly as a fuel and causes engine compatibility issues, such as corrosion, carbon deposition, and thickening of engine lubricants. Therefore, palm oil must be improved through the deoxygenation process by using specific catalysts to be utilized as a biofuel (Ooi *et al*., 2019).

Typically, the triglyceride catalytic cracking reaction pathway is controlled mainly by catalyst properties, such as strength, type and many acid sites, and pore shape (Wang *et al*., 2019). Zhao *et al*. (2015) explained that by using a proper catalyst, catalytic cracking breaks the triglyceride double bonds and removes triglyceride oxygen from palm oil. Research by Kubička *et al*. (2014) showed that the catalytic cracking of palm oil at 300 °C using Si-15NiMo catalyst resulted in a deoxygenation rate of 95% because SiO_2 supports the NiMo catalyst, causing a decarboxylation reaction in the catalytic cracking. Papageridis *et al*. (2020) also reported that the catalytic cracking of palm oil using Ni/Al catalyst showed a deoxygenation rate of 77%. Co-CaO catalyst has bifunctional properties and strong acidic sites on the catalyst generate fatty acid cracking as reported by Asikin-Mijan *et al*. (2016), whilst strong basicity influences deoxygenation pathway in the conversion process of palm oil into hydrocarbons with a deoxygenation rate of 75%. Deoxygenation of triglyceride is a method of removing oxygen atoms contained by fatty acids through decarboxylation ($-CO_2$) and decarbonylation (-CO) and hydrodeoxygenation ($-H_2O$) reactions (Asikin-Mijan *et al*., 2017). However, the decarboxylation and decarbonylation pathways lose each carbon atom to byproducts in the form of CO and CO_2 gases, resulting in the reduction of carbon in the liquid products.

The acid-basic bifunctional catalysts are solid heterogeneous catalysts consisting of both acidic and basic active sites on the catalyst. The advantages of the bifunctional heterogeneous catalysts include their ability to be recycled, reused, and regenerated with minimal energy consumption (Elias *et al*.,

DOI: https://doi.org/10.17509/ijost.v8i2.55494
p- ISSN 2528-1410 e- ISSN 2527-8045

2020). Developing bifunctional catalysts with long lifetimes and high selectivity is the potential to increase the yield of liquid fuel products and reduce the cost. Carbon and hydrogen may also be converted into aromatics and olefins (Istadi *et al*., 2021a; Shakirova *et al*., 1980). Sartipi *et al*. (2014) explained that HY zeolites have more acid sites, which produce stronger acid sites to accelerate cracking. Sugiyama *et al*. (2019) also explained that $CaCO_3$ is used as a catalyst support with a basic site.

Suárez *et al*. (2019) reported that metal impregnation on HY zeolite could enhance the number of Lewis acid sites due to the presence of unpaired electrons in the metals. Metals, such as $CaCO_3$, may be used to modify the characteristics of zeolites to generate Lewis acid sites. Several pathways of hybrid cracking-deoxygenation may occur on $CaCO_3$-modified HY catalysts, including decarboxylation, decarbonylation, and hydrodeoxygenation. These processes may produce carbon dioxide, carbon monoxide, and water as byproducts, respectively.

In biofuel production, oxygen content in the cracking product becomes a problem for fuel cases that must be reduced in the cracking process. According to Kianfar *et al.* (2018), the use of ZSM-5/$CaCO_3$ as a catalytic cracking catalyst improves the production of heavy hydrocarbons by 38.65%. Istadi *et al*. (2021) also found that Ni-Co/HY catalyst supported cracking and deoxygenation mechanisms in the production of biofuels from palm oil reaching a yield of hydrocarbons and oxygenated by 98.46% and 1.54%, respectively. Meanwhile, cracking palm oil using a bifunctional Zn/ZSM-5 catalyst to produce hydrocarbon fuel and oxygen content by 71.78% and 4.07%, respectively, was reported by Zhao *et al*. (2015). Cheng *et al.* (2017) also investigated the hydrodeoxygenation and hydrogenation on the bifunctional Fe-Ni/HZSM-5 catalysts producing the highest biofuel yield of 28.70 wt% and the highest hydrocarbon content of 28.60%.

Although many researchers have reported on many types of suitable bifunctional catalysts for the cracking and deoxygenation of palm oil to biofuels, the specific studies on the design and roles of bifunctional catalysts promote simultaneous cracking and deoxygenation of triglyceride to biofuels are limited. Therefore, it is necessary to develop a bifunctional catalyst that supports simultaneous cracking-deoxygenation of triglyceride to biofuels. The combination of $CaCO_3$ and HY zeolite is expected to increase the acid sites (Lewis and Brønsted acids) and basic sites on the catalysts simultaneously.

However, further detailed testing of the designed $CaCO_3$-modified HY catalyst is required for the catalytic cracking-deoxygenation process of triglyceride into biofuel. To the best of our knowledge, studies on the influence of the bifunctional $CaCO_3$-modified HY catalyst on the simultaneous cracking-deoxygenation reaction pathways were limited. Therefore, this research focused on emphasizing the role of bifunctional the strong acid and strong basic sites generated on the catalyst supporting the simultaneous cracking-deoxygenation of palm oil into diesel-range hydrocarbons.

2. MATERIALS AND METHODS

2.1. Materials

This research used commercial HY zeolite from Zeolyst International (CBV760) as a catalyst support and calcium carbonate (CaCO3) (99.0%, Merck) as a precursor. Palm oil, as a raw material of triglyceride, was used to test the activity of the catalyst in the simultaneous cracking-deoxygenation reactions (**Table 1**). In addition, nitrogen gas (99%, UHP) was used to remove/flush oxygen content in the pipelines and reactor instruments.

DOI: https://doi.org/10.17509/ijost.v8i2.55494
p- ISSN 2528-1410 e- ISSN 2527-8045

Table 1. Fatty acids composition of triglyceride in the palm oil raw material.

No	Component	Chemical Formula	Composition (wt%)
1.	Palmitic acid	C16:0	44.53
2.	Stearic acid	C18:0	1.80
3.	Oleic acid	C18:1	41.91
4.	1-Tridecene	-	5.32
5.	2,6,10,14,18-Penta methyl eicosa pentane	-	6.44
	Total		**100.00**

2.2. Preparation of Catalysts

HY zeolite powder was dried for 1 h at 110 °C in an electric oven (Memmert) and labeled as HY. Then, 20 g of the HY was immersed in a $CaCO_3$ solution (0.25 M). Thus, the targeted impregnated $CaCO_3$ were 5, 10, and 20 wt%. The resulting slurry was stirred at a stirring speed of 600 rpm for 1 h. After that, the slurry was aged overnight. The mixture was filtered and dried overnight at a temperature of 65°C in an electric oven (Memmert) 36. Thus, the targeted $CaCO_3$ content was only physically and chemically adsorbed on the HY catalyst. The catalyst was then calcined at 550°C for 3 h in a furnace (ThermoLyne) and was labeled as $xCaCO_3$/HY catalyst, where x is %wt of $CaCO_3$.

2.3. Catalyst Characterizations

2.3.1. Crystal Structure and Phase Identification of Catalyst Using X-Ray Diffraction (XRD)

Determination of the crystal structure and phase identification of the $CaCO_3$/HY catalyst was conducted using an XRD analysis (Shimadzu 7000) operating at 30 kV and 30 mA with Cu-Kα radiation. The catalyst was scanned at an angle of 2θ from 5-90° at a scanning speed of 3°/min.

2.3.2. Determination of Particle Surface Area and Pore Size Distribution of Catalyst

The adsorption-desorption of the N_2 method (Micromeritics TriStar II 3020) was used to determine the catalysts surface area and pore size distribution. The adsorption of N_2 was conducted at bath temperature of 77 K. Before the adsorption process, catalysts were degassed at 200°C for 2 h. The Brunauer-Emmett-Teller (BET) method was used to determine the specific surface area, while the pore size distribution was determined using the Barrett–Joyner–Halenda (BJH) method.

2.3.3. Catalyst Morphology using Scanning Electron Microscopy – Energy Dispersive X-Ray (SEM-EDX)

SEM-EDX (JEOL JSM-6510LA), 10 µm resolution, and 3,000 to 10,000x magnification were used to examine the morphology of HY, $5CaCO_3$/HY, $10CaCO_3$/HY, and $20CaCO_3$/HY catalysts. At 20 kV, a 1 g powder sample was mounted on a platform and examined for 51.21 sec. Secondary electrons are used to obtain high-resolution SEM images. The elemental composition of solids was determined via EDX analysis by scanning the sample at a precise spot on the specimen.

2.3.4. Acidity Strength using NH_3-Temperature Programmed Desorption (NH_3-TPD)

The catalysts of HY, $5CaCO_3$/HY, $10CaCO_3$/HY, and $20CaCO_3$/HY were weighed as much as 1 g. Samples were pretreated by heating at 350°C for 60 min under He gas (inert). Then, NH_3 adsorption (5% in He, v/v) was carried out at 100 °C for 30 min, then purged with He gas (inert) at the same temperature, for 30 min to remove the physisorbed NH_3. NH_3 desorption was carried out at a temperature of 100–650°C with a temperature increase of 10 °C/min. The entire flow rate of gas is 40 mL/min. The desorbed NH_3 was measured using a thermal conductivity detector (TCD).

DOI: https://doi.org/10.17509/ijost.v8i2.55494
p- ISSN 2528-1410 e- ISSN 2527-8045

2.3.5. Basicity Strength using CO_2 Temperature Programmed Desorption (CO_2-TPD)

Each catalyst of HY, $5CaCO_3$/HY, $10CaCO_3$/HY, and $20CaCO_3$/HY was weighed as much as 1 g. Samples were pretreated by heating at 350°C for 60 min under He gas (inert). The CO_2 adsorption (5% CO_2 in He, v/v) was carried out at room temperature for 30 min, then purged with He gas (inert) at the same temperature for 30 min to remove the physisorbed CO_2. The CO_2 desorption was carried out at room temperature to 650°C with a temperature increase of 10 °C/min. The flow rate of gas is 40 mL/min. The desorbed CO_2 was measured using a thermal conductivity detector (TCD).

2.4. Catalyst Performance Testing and Biofuel Product Analysis

The catalysts were tested for the catalytic cracking-deoxygenation reactions of palm oil over a fixed-bed catalytic reactor (see **Figure 1**) to produce liquid fuels. The reactor was constructed with a stainless-steel tube with a diameter of 1 inch. An electric heating furnace was installed outside the tubing before entering the reactor called a tube line pre-heating process. The catalyst was loaded into the reactor for an amount of 5 g of each run. Then, 100 mL/min of N_2 gas was flowed into the tubing and reactor system for 15 min to flush oxygen gas content within the system. The reactor was heated up to reaction temperature (450 °C) until reach the targeted reactor temperature. After the reactor temperature was steady, palm oil was fed into the reactor at a weight hourly space velocity (WHSV) of 0.288 min^{-1} in which the flow rate was controlled using a peristaltic pump (RZ1030-BX). The product of the reaction was condensed in a condenser equipped with a chiller (CCA-420) and collected as an organic liquid product (OLP) during the cracking process.

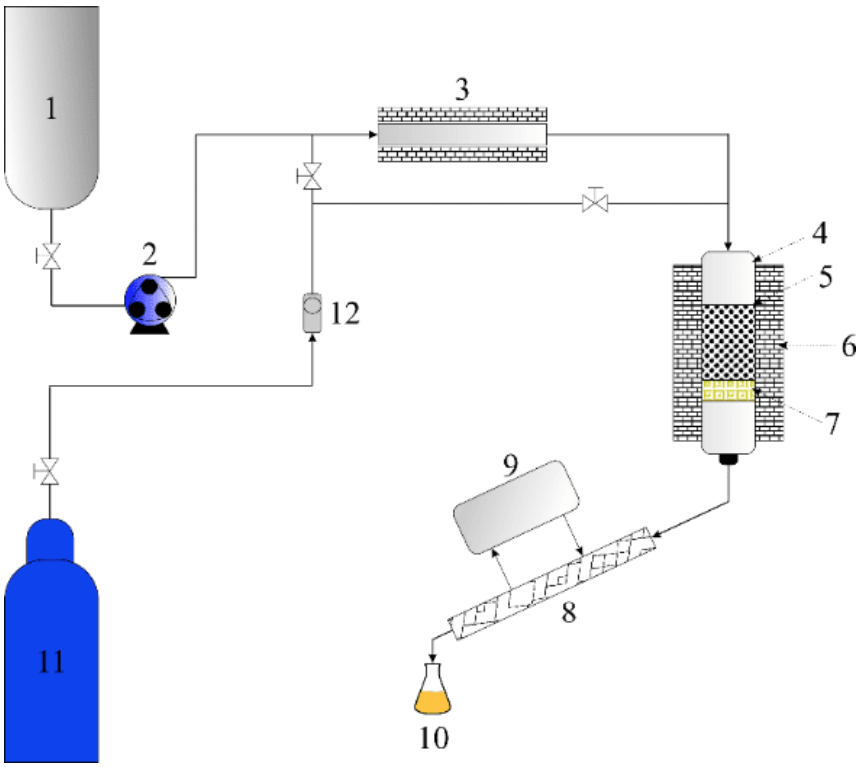

Figure 1. Scheme of continuous catalytic cracking experimental setup: 1) Palm oil tank, 2) Peristaltic pump, 3) Pre-Heater, 4) Fixed-bed reactor, 5) Catalyst bed, 6) Electric Tube Furnace, 7) Glass wool, 8) Condenser, 9) Chiller, 10) Organic liquid product, 11) N_2 gas tank, 12) Flowmeter.

DOI: https://doi.org/10.17509/ijost.v8i2.55494
p- ISSN 2528-1410 e- ISSN 2527-8045

2.5. Product Characterization and Quantification

The organic liquid product (OLP), as a cracking product composed of hydrocarbons and oxygenates, was condensed and collected. The collected liquid product was analyzed using gas chromatography-mass spectrometry (GC-MS). Determination of components identification and compositions of liquid biofuels product was conducted using Gas Chromatography-Mass Spectrometry (GC-MS) (QP2010S SHIMADZU, DB-1 column). The samples were analyzed at 50 °C oven temperature (hold for 5 min) and ramped 10 °C/min to 260 °C and held for 33 min.

The liquid reaction product was taken at the first 3 h after a steady state was achieved for GC-MS analysis purposes. Regarding this matter, an assumption was then taken that the steady state condition was achieved after 30 minutes on stream. To calculate yield and selectivity, the OLP is distilled fractionally based on the temperature range of diesel fraction of 300 – 370 °C (CAS 68334-30-5) using a batch distillation to determine the yield of diesel fraction product. The yield and selectivity were calculated based on Equations (1) – (5).

$$Yield\ of\ OLP\,(\%) = \frac{m_{OLP}}{m_{feed}} \times 100 \quad (1)$$

$$Yield\ of\ gas\,(\%) = \frac{m_{gas}}{m_{feed}} \times 100 \quad (2)$$

$$Yield\ of\ coke\,(\%) = \frac{m_{coke}}{m_{feed}} \times 100 \quad (3)$$

$$Yield\ of\ water\,(\%) = \frac{m_{water}}{m_{feed}} \times 100 \quad (4)$$

$$Selectivity\ of\ diesel\,(\%) = \frac{m_{diesel}}{m_{OLP}} \times 100 \quad (5)$$

3. RESULTS AND DISCUSSION

3.1. Phase Identification and Crystal Structure Analysis using the XRD

The crystal structure of the catalysts (HY, 5$CaCO_3$/HY, 10$CaCO_3$/HY, and 20$CaCO_3$/HY) was determined by utilizing diffraction patterns of XRD analysis. The resulting diffraction peaks were then compared with the ICDD (International Center for Diffraction Data). **Figure 2** and **Table 2** show the diffraction patterns and the analysis of the peak, according to the ICDD3.

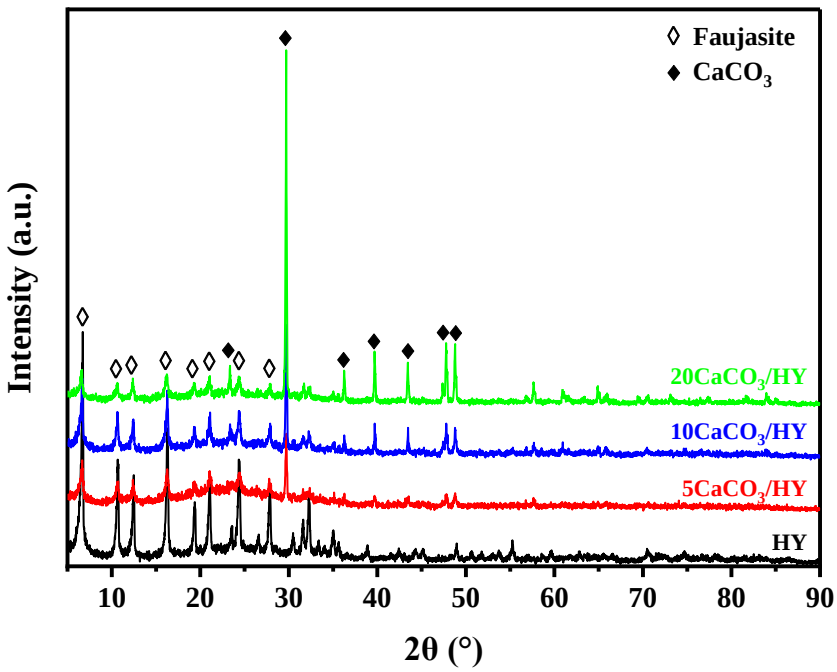

Figure 2. X-ray diffraction patterns of catalysts (HY, 5$CaCO_3$/HY, 10$CaCO_3$/HY, and 20$CaCO_3$/HY).

DOI: https://doi.org/10.17509/ijost.v8i2.55494
p- ISSN 2528-1410 e- ISSN 2527-8045

Table 2. Detected phases of catalysts by ICDD compound data of XRD.

Data	Compound	2θ (°)						
ICDD File	$CaCO_3$[a]	23	29.4	35.5	39.4	43.1	47.5	48.5
	Faujasite[b]	6.2	10.1	11.8	15.6	23.5	-	-
HY	Faujasite	6.6	10.6	12.4	16.2	24.3	-	-
$5CaCO_3$/HY	$CaCO_3$	23.3	29.7	36.2	39.6	43.4	47.7	48.7
	Faujasite	6.6	10.6	12.4	16.2	24.3	-	-
$10CaCO_3$/HY	$CaCO_3$	23.3	29.7	36	39.7	43.1	47.5	48.5
	Faujasite	6.6	10.6	12.4	16.2	24.3	-	-
$20CaCO_3$/HY	$CaCO_3$	23.3	29.7	36.2	39.7	43.4	47.7	48.7
	Faujasite	6.6	10.6	12.4	16.2	24.3	-	-

a COD Database no. 96-900-9668
b COD Database no. 96-154-5416

Based on **Figure 2**, the HY catalyst shows the diffraction peaks with cubic structure (Faujasite) at 2θ of 6.6, 10.6, 12.4, 16.2, and 24.3° concerning hkl of (111), (022), (113), (133), and (335), respectively. These peaks are in line with the result of Choo *et al*. (2020) which identified the diffractogram of the HY zeolite. These peaks were also found in all catalysts (HY, $5CaCO_3$/HY, $10CaCO_3$/HY, and $20CaCO_3$/HY), indicating that the Faujasite structure is found in all catalysts. The diffraction peaks of $CaCO_3$ with a hexagonal structure are detected at 2θ of 23.3, 29.6, 36.2, 39.6, 43.4, 47.4, and 48.7° concerning hkl of (102), (104), (110), (113), (202), (018) and (116), respectively. The presence of these diffraction peaks indicates that the $CaCO_3$ has been impregnated successfully on the HY catalyst.

As shown in **Figure 2**, the diffraction pattern of $CaCO_3$ increases as the rising amount of impregnated $CaCO_3$. It indicates that the presence of the hexagonal structure of the $CaCO_3$ phase increases. However, the peak of the Faujasite structure decreases with the increase in $CaCO_3$ concentration. The decreases in the peaks' intensity could be caused by the decrease in the relative crystallinity and/or the X-ray absorption by the metals (Huang *et al*., 2017) In addition, the phase interpretation of the detected XRD peaks also indicates that the $CaCO_3$ was not converted to CaO during the calcination process (calcination temperature of 550°C). **Table 2** shows the peaks analysis of HY, $5CaCO_3$/HY, $10CaCO_3$/HY, and $20CaCO_3$/HY catalysts and compares them with ICDD (International Center for Diffraction Data).

3.2. Surface Area, Pore Volume, and Pore Size Properties of Catalysts

The catalysts were characterized by their surface area and pore size distribution using the N_2 adsorption method and estimated using procedures of Brunauer-Emmett-Teller (BET) and Barret-Joyner-Halenda (BJH), respectively. The N_2 adsorption characterization method was performed on HY, $5CaCO_3$/HY, $10CaCO_3$/HY, and $20CaCO_3$/HY catalysts to determine their surface area, pore volume size, and pore size distribution.

Figure 3(A) shows that all catalysts have the type IV isotherm profile of an N_2 isotherm-adsorption, indicating the presence of microporous and mesoporous structures (Al-Othman, 2012). In **Figure 3(A)**, all catalysts tend to dip upwards at low p/po (p/po < 0.01), which is attributed to the micropores filling. However, this dip upward is significantly decreased as the increase in the $CaCO_3$ addition. It indicates that the micropores composition is decreased. It is true since the micropore volume (V_{micro}) is significantly decreased after $CaCO_3$ addition (**Table 3**).

DOI: https://doi.org/10.17509/ijost.v8i2.55494
p- ISSN 2528-1410 e- ISSN 2527-8045

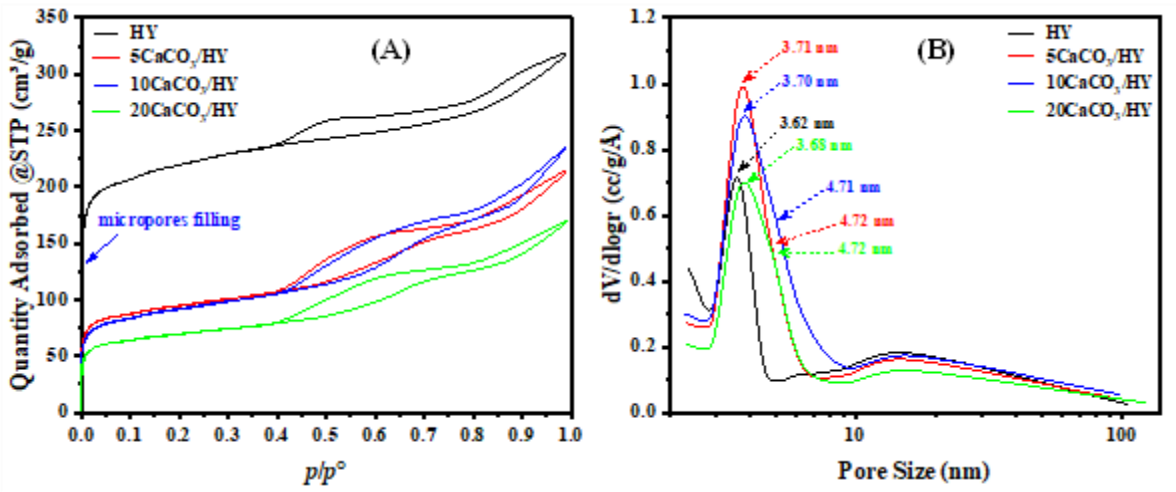

Figure 3. (A) N_2-sorption isotherm and (B) pore size distribution of the catalysts.

Table 3. Characterization of surface area, pore volume, and pore size of the catalysts.

Catalysts	S_{BET} (m^2/g)	S_{micro}* (m^2/g)	S_{ext}* (m^2/g)	d_p‡ (nm)	V_{micro}* (cm^3/g)	V_{total} (cm^3/g)
HY	687	490	197	3.62	0.252	0.492
$5CaCO_3$/HY	307	149	158	3.71	0.077	0.362
$10CaCO_3$/HY	299	130	169	3.70	0.067	0.331
$20CaCO_3$/HY	226	105	121	3.66	0.054	0.262

*Based on t-plot method; ‡Average pore size using BJH-desorption data

From **Table 3**, the effect of adding $CaCO_3$ to the HY zeolite catalyst is indicated, which causes a decrease in surface area and pore volume by 226 m^2/g and 0.262 cm^3/g, respectively. The decreased surface area is caused by the metal agglomeration of $CaCO_3$, while the decrease in the pore volume of the catalyst was caused by the micropore filling by $CaCO_3$ particles during the impregnation process (Liu & Corma, 2018). According to research by Wang *et al*. (2020) the addition of $CaCO_3$ results in a reduction in surface area and pore volume, which is consistent with the results in this investigation. It is conceivable for an uneven metal distribution on the catalyst surface to occur during the impregnation process when a relatively high metal concentration causes ion competition near the pore opening (Anggoro *et al*., 2017). Tsai (2013) also explained that $CaCO_3$ particles have poorer pore properties than nitrogen probes and porous materials such as zeolites. They suggested that the addition of $CaCO_3$ into HY zeolite decreases the surface area and pore volume because of the pore filling.

Figure 3(B) shows the pore size distribution of HY, $5CaCO_3$/HY, $10CaCO_3$/HY, and $20CaCO_3$/HY catalysts. The higher content of $CaCO_3$ added to the HY catalyst decreases the catalyst surface area, because some micropores were blocked by $CaCO_3$. However, Cheng *et al.* (2022) explained that the size of the pores can be controlled by applying $CaCO_3$. Catalysts with mesoporous pore sizes have the advantage of adjusting the hydrocarbon distribution's porosity and acidity (Jun *et al*., 2017). Therefore, the addition of $CaCO_3$ can increase the acidity (Lewis acid site) of the catalyst to produce the desired liquid fuel product (Kianfar *et al*., 2018). Lewis acid site is provided by empty orbitals which can accept electron pairs. Introducing transition metal on zeolite provides orbital which consists of a single electron in d orbital as active sites to homolytically dissociate hydrogen gas in a

DOI: https://doi.org/10.17509/ijost.v8i2.55494
p- ISSN 2528-1410 e- ISSN 2527-8045

hydrocracking reaction. Munnik *et al*. (2015) found that the catalyst impregnation process mixture produced an aggregation on the catalyst surface. Based on this finding related to the aforementioned literature, during the impregnation process with $CaCO_3$, the macropore structure fills up on the catalyst's surface, which makes the mesoporous structure bigger. Therefore, the addition of $CaCO_3$ to the HY impregnation caused a decrease in the surface area and pore volume (**Table 3**), which was caused by covering the pores of HY zeolite with $CaCO_3$ particles. In addition, the impregnation process causes the formation of agglomerations of metal particles on the catalyst surface which can increase the pore sizes.

3.3. Morphology Analysis of Catalysts Using SEM-EDX

The SEM characterization was used to analyze the surface morphology and pore size distribution of the catalysts, while the elemental composition in the catalysts was analyzed using EDX. **Figure 4** shows the findings of SEM characterization for HY, $5CaCO_3$/HY, $10CaCO_3$/HY, and $20CaCO_3$/HY catalysts. **Figure 4(A)** shows the SEM morphology of the original HY catalyst, which looks homogeneous, the crystallinity is sharper, and the morphological structure is cubic crystals with a particle size of 800±175 nm. Oyebanji *et al.* (2020) identified zeolite-Y with a similar particle size distribution as this study. Research by Oenema *et al*. (2020) also suggested that zeolite-Y crystal size is between 200-1000 nm. **Figure 4(B-D)** shows the catalysts of $5CaCO_3$/HY, $10CaCO_3$/HY, and $20CaCO_3$/HY with a hexagonal structure that produces an average particle size of 673±190 nm, 654±160 nm, and 770±211 nm, respectively. Because of the covering catalyst surface by aggregate, the addition of more $CaCO_3$ causes an increase in the particle size of the catalyst, leading to an uneven particle size distribution on the catalyst (**Table 3**). Doyle *et al*. (2016) postulated that contaminants in HY zeolite may have contributed to the agglomeration. The aggregate particles on $CaCO_3$/HY are formed from interconnected cubic and hexagonal structures. This was also confirmed by XRD analysis results (**Figure 2**), which revealed the formation of HY with a cubic structure and $CaCO_3$ with a hexagonal structure.

The energy dispersive X-ray (EDX) was used to determine the elemental composition of catalysts (HY, $5CaCO_3$/HY, $10CaCO_3$/HY, and $20CaCO_3$/HY), after being calcined at a temperature of 550 °C for 3 hours, while the composition results are tabulated in **Table 4**. Based on **Figure 5**, the EDX results of the HY catalyst contains the elements of Si, Al, Cu, and O, while the $5CaCO_3$/HY, $10CaCO_3$/HY, and $20CaCO_3$/HY catalysts contain Si, Al, Ca, Cu, and O.

The presence of calcium in $CaCO_3$/HY catalysts suggests that $CaCO_3$ was successfully impregnated on the HY catalyst, owing to the distribution of Ca metal inside the HY zeolite structure which is also confirmed by XRD characterization. Furthermore, the Si/Al ratios of HY, $5CaCO_3$/HY, $10CaCO_3$/HY, and $20CaCO_3$/HY catalysts are 26.08, 29.76, 20.04, and 24.78, respectively.

The increased Si/Al ratio changes the acidic zeolite characteristics, resulting in a reduction in the concentration of Brønsted acid sites (Golubev *et al*., 2021). However, Doyle *et al*. (2016) stated that the increase in the Si/Al ratio of zeolite over 2.5–10.0 increased the strength of Brønsted acid, the hydrophobicity of the catalyst, and the number of acid sites. Meanwhile, the Lewis acid site also increases with increasing Si/Al ratio (Hartanto *et al*., 2016). **Table 4** clearly shows that an increase in Al content during the $CaCO_3$ impregnation on HY zeolite caused a lower Si/Al ratio, especially for $10CaCO_3$/HY and $20CaCO_3$/HY catalysts. However, the $CaCO_3$-modified catalysts had a higher Si/Al ratio than the original HY zeolite, because some Brønsted acid site protons of HY zeolite were substituted by Ca^{2+} or the aluminum species is moved to extra-framework, resulting in a larger concentration of Lewis acid sites.

DOI: https://doi.org/10.17509/ijost.v8i2.55494
p- ISSN 2528-1410 e- ISSN 2527-8045

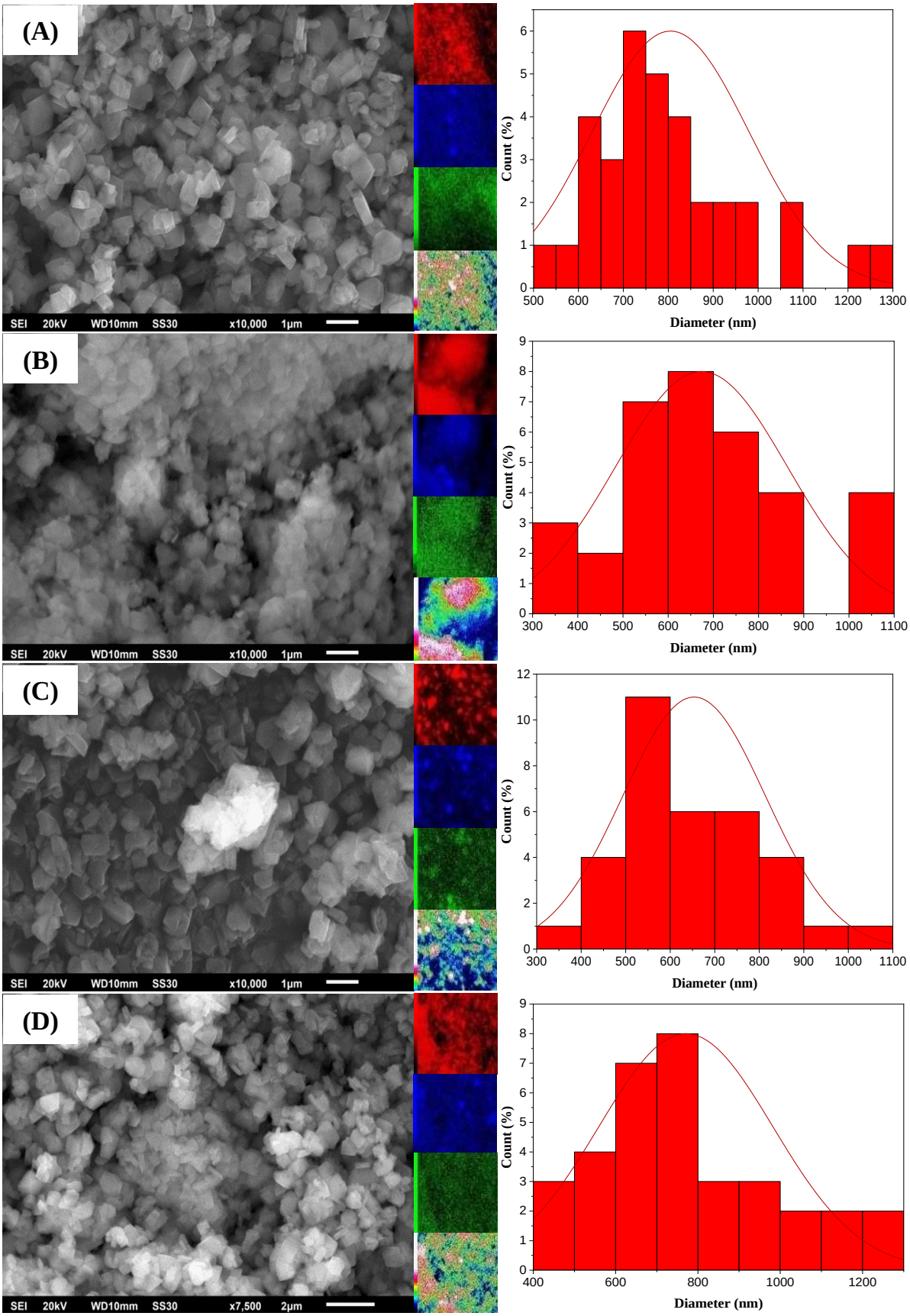

Figure 4. SEM characterization results of catalysts: (A) HY, (B) 5$CaCO_3$/HY, (C) 10$CaCO_3$/HY, dan (D) 20$CaCO_3$/HY.

DOI: https://doi.org/10.17509/ijost.v8i2.55494
p- ISSN 2528-1410 e- ISSN 2527-8045

Table 4. Elemental composition of catalysts analyzed by EDX.

Elemental Composition	HY (% mass)	5$CaCO_3$/HY (% mass)	10$CaCO_3$/HY (% mass)	20$CaCO_3$/HY (% mass)
O	79.13	64.58	69.01	81.18
Al	0.74	1.09	1.12	0.77
Si	19.24	32.50	27.76	15.38
Ca	0.00	0.85	1.26	1.35
Cu	0.88	0.99	0.85	1.30
Si/Al Ratio	26.08	29.76	24.78	20.04

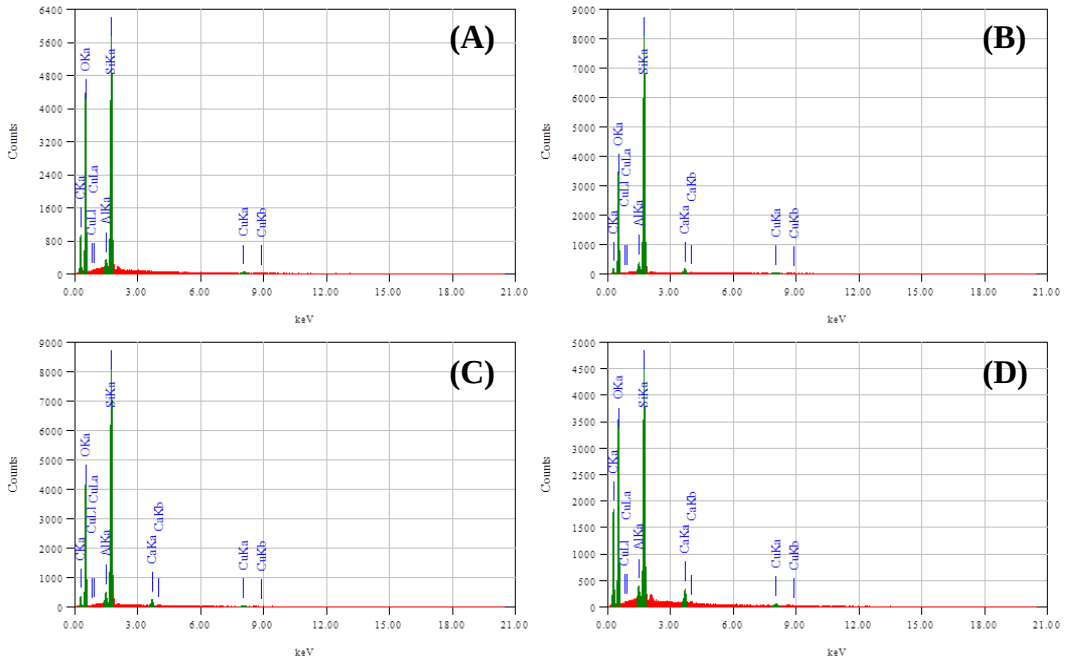

Figure 5. Elemental composition of catalysts: (A) HY, (B) 5$CaCO_3$/HY, (C) 10$CaCO_3$/HY, and (D) 20$CaCO_3$/H.

3.4. Analysis of Acidity and Basicity Strengths using NH_3- and CO_2- probed Temperature Programmed Desorption (TPD)

The acid and basic strengths of catalysts were determined using NH_3-TPD and CO_2-TPD methods, respectively, because of $CaCO_3$ impregnation on HY zeolite (**Figure 6** and **Table 5**). According to Yi *et al*. (2019), there were three kinds of adsorbed species on alkaline metal oxide basic sites through CO_2-TPD, including unidentate carbonate forms on surface O^{2-} ions, bidentate carbonate forms on Lewis-acid–Brønsted-basic pairs (Ca^{2+}–O^{2-}), and bicarbonate species on weak basic sites. Concerning the cracking process, the Brønsted acid site is important according to Meng *et al*. (2022) suggestion that the reaction conversion and product distribution of the cracking process may be controlled by adjusting the Brønsted acidity of zeolite HY. In general, a strong acid catalyst with a high concentration of Brønsted and/or Lewis acids sites of original or modified zeolite HY is needed for cracking hydrocarbon, while deoxygenation reaction pathway is tailored by strong basicity adjusted by $CaCO_3$. Based on the desorption temperature of NH_3, the acid strength of NH_3-TPD is classified as weak (120–300 °C), moderate (300–500 °C), and strong (>500 °C) acid sites (Suprun *et al*., 2009). Meanwhile, CO_2-TPD-based basic strength is classified as weak (50–200 °C), moderate (200–400 °C), and strong (>400 °C) basic sites (Ezeh *et al*., 2018).

DOI: https://doi.org/10.17509/ijost.v8i2.55494
p- ISSN 2528-1410 e- ISSN 2527-8045

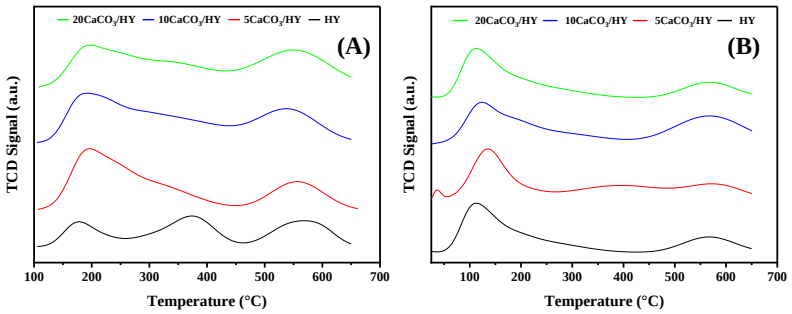

Figure 6. Catalysts characterization results of acid and basic strengths using: (A) NH_3-TPD and (B) CO_2-TPD of catalysts.

Table 5. Concentration distribution of acid and basic sites of catalysts based on the range of acidity and basicity strengths.

Catalyst	NH_3-TPD (µmol/g)			Total Acid Sites (µmol/g)	CO_2-TPD (µmol/g)			Total Basic Sites (µmol/g)
	Weak	Moderate	Strong		Weak	Moderate	Strong	
HY	119	242	197	558	124	28	48	200
5$CaCO_3$/HY	401	348	249	998	195	141	66	402
10$CaCO_3$/HY	370	246	259	875	211	115	215	541
20$CaCO_3$/HY	226	284	323	833	387	93	139	619

Figure 6 and **Table 5** present the results of the NH_3-TPD and CO_2-TPD analysis of the catalysts. **Figure 6(A)** shows that the total acid site concentrations of the HY, 5$CaCO_3$/HY, 10$CaCO_3$/HY, and 20$CaCO_3$/HY catalysts are 558, 998, 875, and 833 µmol/g, respectively. The NH_3-TPD results suggest that adding $CaCO_3$ to the HY catalyst changes the acid strength of the catalyst, especially the strong acid site. As presented in **Table 5**, the addition of $CaCO_3$ increases the formation of strong acid sites, but it slightly appears in **Figure 6(A)**. It suggested that this acidity comes from the Lewis acid site of Ca^{2+} from the bidentate carbonate which is in line with the results of Yi *et al*. (2019). Furthermore, the change in the acid strength of catalysts affects the surface catalytic activity, especially for the cracking reaction pathway. Zheng *et al.* (2021) and Putluru *et al.* (2011) explained that the weak acidity of zeolite-based materials is mainly attributed to the Brønsted acid site, while moderate and strong acidities are attributed to the Lewis acid site. In addition, Huang *et al.* (1991) also explained that calcium carbonate on the catalyst surface is the dominating surface site and acts as a Lewis acid site. Based on these understandings, it is suggested that the strong acidity after $CaCO_3$ addition to HY catalyst is attributed to the formation of the Lewis acid site. Moreover, the addition of $CaCO_3$ on zeolite enhances Lewis acid sites rather than Brønsted acid sites from HY.

Table 5 shows that the total basic sites of the catalysts of HY, 5$CaCO_3$/HY, 10$CaCO_3$/HY, and 20$CaCO_3$/HY are 200, 402, 541, and 619 µmol/g, respectively. In the catalysts, the adsorbed CO_2, which is desorbed at a low-temperature range, indicates weak basicity, while the adsorbed CO_2, which is desorbed at higher temperature ranges, indicates moderate and strong basicity (Charisiou *et al.*, 2018). Concerning the $CaCO_3$ doped on HY catalyst characterization results, Dias & Assaf (2003) also explained that Ca^{2+} ions may enhance the ion density of the basic site of the catalyst leading to increased CO_2 adsorption, which can support the decarboxylation reaction pathway of fatty acids. In addition, the strong basic site plays a role in maintaining the stability of the catalyst and causes an increase in the activity of the catalyst concerning the deoxygenation reaction (Asikin-Mijan *et al.*, 2020; Wei *et al.*, 2003).

DOI: https://doi.org/10.17509/ijost.v8i2.55494
p- ISSN 2528-1410 e- ISSN 2527-8045

The high-temperature range of the CO_2 desorption peak (> 400°C) of the CO_2-TPD analysis demonstrated a relatively high basic strength of the designed catalysts. The presence of $CaCO_3$ on the surface of the HY zeolite modifies the zeolite's surface structure which in turn has an impact on the acidity and basicity of the catalyst. After physically interacting with the neighboring Ca^{2+} ion, the CO_3^{2-} ion gets polarized and forms monodentate carbonate. Monodentate carbonate attacks the oxygen atom that binds aluminum and silicon, puncturing the aluminum-oxygen bond and forming Lewis acid sites. Additionally, the O^{2-} ions that are neighboring the Ca^{2+} ions are polarized and fill the aluminum structure's lone pair. Furthermore, Ca^{2+} ions attack the electrons of aluminum, resulting in the formation of Brønsted acid sites (Bonenfant *et al.*, 2008; Gallei & Stumpf, 1976). Moreover, the basic site which is adsorbed through the Lewis acid - Brønsted basic pair ($Ca^{2+} – O^{2-}$) produces a weak basic site (Yi *et al.*, 2019; Puriwat *et al.*, 2010).

3.5. Catalyst Performance Testing for Cracking Palm Oil Process to Diesel-Range Hydrocarbons

The HY, $5CaCO_3$/HY, $10CaCO_3$/HY, and $20CaCO_3$/HY catalysts were tested for cracking palm oil to produce liquid fuels (especially diesel-range hydrocarbons). The blank test at 450 °C was also included. The blank test was conducted at the same feed flow rate as the catalytic test. As presented in **Figure 7**, the utilization of catalysts slightly increases the yield of organic liquid product (OLP). In addition, the yield of OLP as the addition of $CaCO_3$ on HY catalysts is comparable. Using the catalysts of HY, $5CaCO_3$/HY, $10CaCO_3$/HY, and $20CaCO_3$/HY, the OLP yields were found to be 77.41, 79.09, 77.53, and 76.53%, respectively. Higher $CaCO_3$ concentration in the catalysts enhances the mesoporous structure by covering the micropore pores with $CaCO_3$ aggregates which reduces surface area and pore volume, which results in the filling and blocking of micropores in the HY zeolite.

This is due to the addition of calcium carbonate producing more mesopore (see **Table 3**). According to Twaiq *et al.* (2004), the increase in concentrations and strengths of acidic sites might result in over-cracking, resulting in a decrease in OLP production. In contrast, increasing the concentration of $CaCO_3$ in the catalysts enhances the acidity and basicity of the catalyst (**Figure 6**). As seen in **Figure 7**, the production of gas as calculated from mass balance increases as the $CaCO_3$ concentration increases. The gas yields for the usage of HY, $5CaCO_3$/HY, $10CaCO_3$/HY, and $20CaCO_3$/HY catalysts are 18.46, 17.57, 16.72, and 18.03%, respectively.

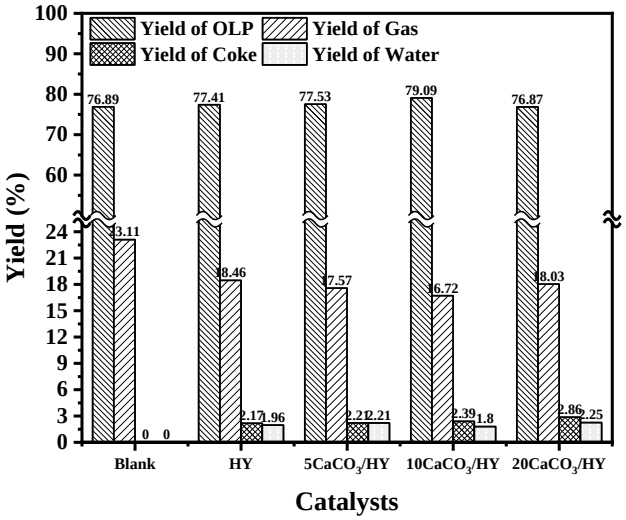

Figure 7. Catalyst testing results for cracking palm oil to biofuels.

DOI: https://doi.org/10.17509/ijost.v8i2.55494
p- ISSN 2528-1410 e- ISSN 2527-8045

Concerning coke formation during the cracking-deoxygenation process, the yields of coke formed on the catalysts of HY, 5$CaCO_3$/HY, 10$CaCO_3$/HY, and 20$CaCO_3$/HY are 2.17, 2.21, 2.39, and 2.86%, respectively. It shows that the highest coke yield is found by the 20$CaCO_3$/HY catalyst. It was reported that the optimum reaction temperature for chain scission of C=O in free fatty acids is between 350 and 375°C. Thus, the reaction temperature above 400 °C results in the creation of coke due to the enhanced cracking process (Ramesh *et al.*, 2019; Khan *et al.*, 2019). In addition, as shown in **Table 3**, the surface area of the catalysts decreases and the average pore size increases as the increases of $CaCO_3$ amount.

The $CaCO_3$ aggregates cover the macropore size on the catalyst surface, increasing the mesopore structure and coke in the catalytic cracking process.Therefore, the surface area and pore size of the catalyst could affect coke formation. In addition, the highest strong acid site is shown on the 20$CaCO_3$/HY catalyst (**Figure 6**). It is well-known that the strong acid site enhances the cracking reaction pathway performance as well as coking formation. It was reported that coke increased due to the strong acidity of the catalyst, especially Lewis acid, which caused the cracking reaction (Istadi *et al.*, 2021a). Therefore, the coke formation is affected by both surface area and acid site amount. Furthermore, the yield of water over the usage of the 5$CaCO_3$/HY, 10$CaCO_3$/HY, and 20$CaCO_3$/HY catalysts, which are 1.96%, 2.21%, 1.80%, and 2.25 %, respectively, suggests an enhanced deoxygenation (hydrodeoxygenation) reaction as also supported by Hermida *et al.* (2015) in which water yield is due to the water-gas shift reaction (WGSR) during the deoxygenation process. However, the blank test does not produce water. It indicates that the deoxygenation reaction might not occur.

Indeed, the catalyst performance test results presented show that increasing $CaCO_3$ concentration from 5% to 20% (w/w) doped on the HY zeolite catalyst slightly increases the yield of gaseous products, coke, and water, but slightly decreased the yield of OLP or biofuel product. Overall, this indicated that the cracking activity of the HY zeolite is slightly higher than that of the $CaCO_3$/HY. The triglyceride molecules are catalytically cracked at the catalyst surface, resulting in heavier hydrocarbons and oxygenated chemicals, such as fatty acids, ketones, aldehydes, and esters. Additionally, secondary cracking converts the intermediate compounds into gaseous products (CO, CO_2, H_2), paraffin, and olefins with long and short chains, water, and alcohols.

3.6. Effect of $CaCO_3$ Modification of HY Catalyst on Hydrocarbons Composition Distribution of Biofuels in the OLP Product

The hydrocarbon composition distribution in the OLP biofuel product is analyzed using Gas Chromatography-Mass Spectrophotometer (GC-MS) and reported in **Figure 8**. **Figure 8** explains the results of the catalyst performance test over the catalytic cracking-deoxygenation of palm oil. In this catalytic reaction test, hydrocarbons-based fuel product is increased from 91.14% to 94.56% because of the introduction of $CaCO_3$ on the HY catalyst (20$CaCO_3$/HY), while the composition of an oxygenated compound of biofuel decreased from 8.85 to 5.48%. The detailed components of the OLP are presented in **Table 6** based on GC-MS analysis. The oxygen atom content of the liquid biofuel product decreases significantly when using 20$CaCO_3$/HY catalyst from 0.91 to 0.05%. This acid site supports the cracking and deoxygenation reaction pathways, while the high basic strength (**Figure 6(B)**) enhances the deoxygenation reaction mechanism including decarboxylation and decarbonylation. These bifunctional roles of catalyst remove more oxygen atoms from palm oil as CO_2 and CO molecules through the decarboxylation and decarbonylation reaction pathways, respectively.

DOI: https://doi.org/10.17509/ijost.v8i2.55494
p- ISSN 2528-1410 e- ISSN 2527-8045

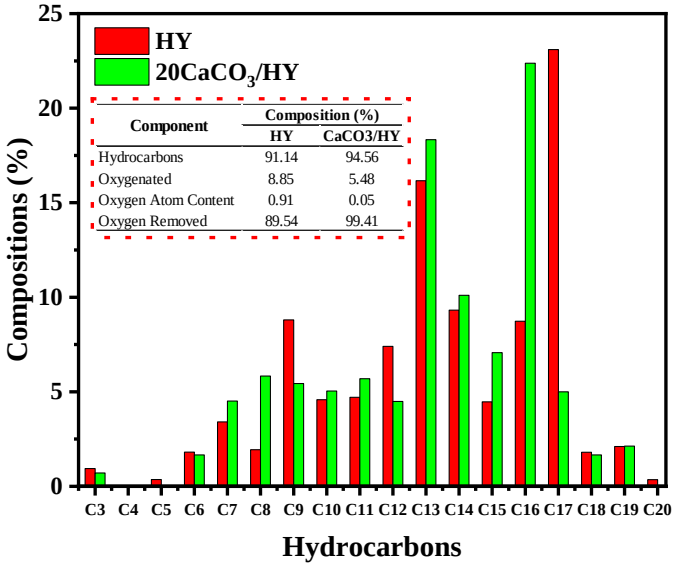

Figure 8. Composition distribution of hydrocarbon products (wt%) of Organic Liquid Product.

Table 6. Composition of OLP by GC-MS analysis.

Components	Molecular Formula	Composition (wt%)	
		HY Catalyst	20$CaCO_3$/HY Catalyst
Hydrocarbons		***91.14***	***94.56***
Cyclopentene	C_5H_8	0.36	-
Cyclohexene	C_6H_{10}	0.33	0.28
1-Hexene	C_6H_{12}	0.53	0.4
Hexane	C_6H_{14}	0.95	0.98
1-Heptene	C_7H_{14}	1.67	2.11
Heptane	C_7H_{16}	1.74	2.4
1-Octene	C_8H_{16}	1.94	2.35
Octane	C_8H_{18}	-	3.48
3-Octyne, 2-methyl	C_9H_{16}	0.39	0.77
Cyclohexene, 3-propyl	C_9H_{16}	0.29	-
1-Nonene	C_9H_{18}	1.9	1.76
Heptane, 2-4 Dimethyl	C_9H_{20}	2.83	-
Nonane	C_9H_{20}	3.39	2.91
Benzene, 2-ethenyl-1,4-dimethyl	$C_{10}H_{12}$	-	0.35
Cyclohexene, 3-(2-methylpropyl)	$C_{10}H_{18}$	-	0.3
Cyclopentene, 1-(3-Methylbutyl)	$C_{10}H_{18}$	0.24	-
1-Decene	$C_{10}H_{20}$	1.37	1.47
Cis-3-Decene	$C_{10}H_{20}$	0.3	-
Decane	$C_{10}H_{22}$	2.02	2.06
Benzene, pentyl	$C_{11}H_{16}$	0.43	-
Cyclohexene, 1-Pentyl	$C_{11}H_{20}$	-	1.79
Cyclopropane, 1-pentyl-2-propyl	$C_{11}H_{22}$	1.89	1.54
5-Undecene	$C_{11}H_{22}$	0.22	-
Undecane	$C_{11}H_{24}$	2.17	2.36
Cyclopropane, Nonyl	$C_{12}H_{24}$	1.61	1.81
1-Dodecene	$C_{12}H_{24}$	1.97	2.19
2-Dodecene	$C_{12}H_{24}$	0.44	-
3-Dodecene	$C_{12}H_{24}$	-	0.49
Dodecane	C12H26	3.38	-
Benzene, heptyl	C13H20	-	0.37
1-Tridecene	C13H26	4.26	5.06

DOI: https://doi.org/10.17509/ijost.v8i2.55494
p- ISSN 2528-1410 e- ISSN 2527-8045

Table 6 (Continue). Composition of OLP by GC-MS analysis.

Components	Molecular Formula	Composition (wt%)	
		HY Catalyst	20$CaCO_3$/HY Catalyst
Tridecane	$C_{13}H_{28}$	6.65	10.44
Cyclotetradecane	$C_{14}H_{28}$	1.17	1.65
Tetradecane	$C_{14}H_{30}$	8.15	8.16
Cyclopentane, decyl	$C_{15}H_{30}$	1.3	0.98
1-Pentadecene	$C_{15}H_{30}$	1.89	5.23
Cyclopentadecane	$C_{15}H_{30}$	0.55	0.58
Cyclohexene, 1-Decyl	$C_{16}H_{30}$	1.9	0.67
3-Hexadecene	$C_{16}H_{32}$	1.37	0.95
Cyclohexadecane	$C_{16}H_{32}$	-	0.34
Hexadecane	$C_{16}H_{34}$	4.53	19.54
Cyclohexane, undecyl	$C_{17}H_{34}$	1.18	1.12
1-Heptadecene	$C_{17}H_{34}$	5	1.74
8-Heptadecene	$C_{17}H_{34}$	-	2.14
Heptadecene	$C_{17}H_{36}$	16.92	-
1-Octadecene	$C_{18}H_{36}$	1.17	1.66
9-Octadecene	$C_{18}H_{36}$	0.63	
1-Nonadecene	$C_{19}H_{38}$	2.11	2.13
Aldehyde		**0.94**	**0.71**
2-Propenal	C3H4O	0.94	0.71
Ketone		***0.36***	***0.86***
Tetracyclo [3.3.1.0.1(3,9)]decan-10-one	$C_{10}H_{12}O$	-	0.42
2-Decanone	$C_{10}H_{20}O$	0.36	0.44
Acids		***0.29***	***0.28***
Decanoic Acid	$C_{10}H_{20}O_2$	0.29	-
Propandioic acid, dicyclohexyl ester	$C_{15}H_{24}O_4$	-	0.28
Alcohol		***7.26***	***3.63***
1-Tridecanol	$C_{13}H_{28}O$	5.25	2.46
1-Tetradecanol	$C_{14}H_{30}O$	-	0.29
1-Pentadecanol	$C_{15}H_{32}O$	0.73	-
1-Hexadecanol	$C_{16}H_{34}O$	0.93	0.88
1-Eicosanol	$C_{20}H_{42}O$	0.35	-

Concerning the HY and 20$CaCO_3$/HY catalysts showing 91.14 and 94.56% hydrocarbon contents, respectively, although the catalyst surface area decreases (**Table 3**) significantly, the pore size of catalysts increases from 2.86 to 4.62 nm due to $CaCO_3$ introduction shifting to the heavier hydrocarbons range products (diesel range rather than gasoline range). However, the $CaCO_3$ introduction on the HY catalyst may affect the Lewis acid sites in improving the hydrocarbon yield (Phung *et al*., 2013). Based on Kianfar *et al*. (2018) results, the addition of $CaCO_3$ into ZSM-5 zeolite caused a decrease in surface area and increased heavy hydrocarbons by 38.65%, which is in line with this study's results. Asikin-Mijan *et al*. (2017) also found that the Co-CaO catalyst has high catalytic activity in the deoxygenation reaction, resulting in a hydrocarbon product with a C_{15}+C_{17} chain of 54%.

The presence of palm oil short-chain hydrocarbons (C_3–C_{14}) suggests a hybrid role of cracking-deoxygenation reaction pathways. The deoxygenation reaction pathway eliminated the carboxyl and carbonyl groups in the fatty acid, resulting in a hydrocarbon with one atom less carbon than the parent structure (C_{16} and C_{18}). The cracking-deoxygenation reaction requires more Brønsted and Lewis acids sites (higher acidity strength), while the deoxygenation reaction

DOI: https://doi.org/10.17509/ijost.v8i2.55494
p- ISSN 2528-1410 e- ISSN 2527-8045

pathway is enhanced by the higher basicity strength due to the role of $CaCO_3$ introduction to HY to attract adsorption of CO_2 and CO of the fatty acids. Therefore, these designed catalysts ($CaCO_3$/HY) have the bifunctional roles required in cracking-deoxygenation reaction mechanisms. From the cracking-deoxygenation reaction mechanisms, some gases were also formed in these findings, i.e. carbon dioxide (CO_2) from the decarboxylation reaction pathway, carbon monoxide (CO) from the decarbonylation reaction pathway, and H_2O from the hydrodeoxygenation reaction pathway due to role of self-produced hydrogen (H_2) (from WGS reaction or dehydrogenation from fatty acids or hydrocarbons) in the reaction.

Based on the GC-MS results (**Figure 8**), it is possible to shift cracking performance to lower chain (C_{16} hydrocarbon) product when using the 20$CaCO_3$/HY catalyst through β-scission of C–C as also suggested by Santillan-Jimenez & Crocker (2012). In this case, the oxygenated compounds, formed by catalytic cracking, diffuse into the pores of the $CaCO_3$-modified HY catalysts and react with protons at the active sites through multiple reaction pathways, such as decarboxylation, decarbonylation, and hydrodeoxygenation. Therefore, the $CaCO_3$ impregnated on the HY catalyst has bifunctional effects of the catalyst supporting cracking-deoxygenation reaction mechanisms as mentioned previously. The role of 20$CaCO_3$/HY as a bifunctional acid-basic catalyst is attributed to its higher activity in deoxygenation and cracking reaction mechanisms.

3.7. Effect of $CaCO_3$ Modification of HY Zeolite Catalyst on Hydrocarbons Product Selectivity

The effect of $CaCO_3$-modified catalysts on hydrocarbon (diesel) fuel product selectivity is presented in **Figure 9**. In the blank test, the selectivity of the diesel fraction was different, which was much lower than in a catalytic test. However, the obtained diesel fraction is dominated by fatty acid because it is coagulated rapidly at room temperature.

The utilization of catalysts significantly increases the selectivity of diesel fraction. In addition, according to **Figure 9**, the doping $CaCO_3$ on the HY catalyst increases diesel-range hydrocarbon product selectivity from 28.4 to 31.88 %. Compared to the other previous research on palm oil cracking, this study produces more diesel hydrocarbon fraction (**Table 7**).

This result demonstrates a synergistic effect of $CaCO_3$ introduction and HY roles, which results in good selectivity in the short-chain hydrocarbons fraction and high activity in the cracking and deoxygenation reactions mechanism simultaneously. Furthermore, the significant activities of cracking and deoxygenation (decarboxylation, decarbonylation, and hydrodeoxygenation) were enhanced by the high-strength acidity and basicity effects on the catalyst (**Figure 6**). In this case, the high acidity strength promotes the diesel selectivity, whereas the high strength of basicity leads to the deoxygenation reaction.

The improvement in selectivity to diesel range hydrocarbons was caused by a larger pore size (**Table 3**). Fathi *et al.* (2014) also reported that the addition of $CaCO_3$ on the HZSM-5 improved selectivity to gasoline. They also reported that high selectivity of diesel towards short-chain hydrocarbon fraction was observed when using HY and modified-$CaCO_3$. It was also reported that the diesel range hydrocarbon selectivity can be affected by the mesoporous distribution of the catalyst (Peng *et al.*, 2015). Based on **Figure 3(B)**, the 20$CaCO_3$/HY has a larger pore size than the HY zeolite, which means that the impregnation of $CaCO_3$ on the HY catalysts enhances the average pore size of the catalysts, although the surface area decreases.

DOI: https://doi.org/10.17509/ijost.v8i2.55494
p- ISSN 2528-1410 e- ISSN 2527-8045

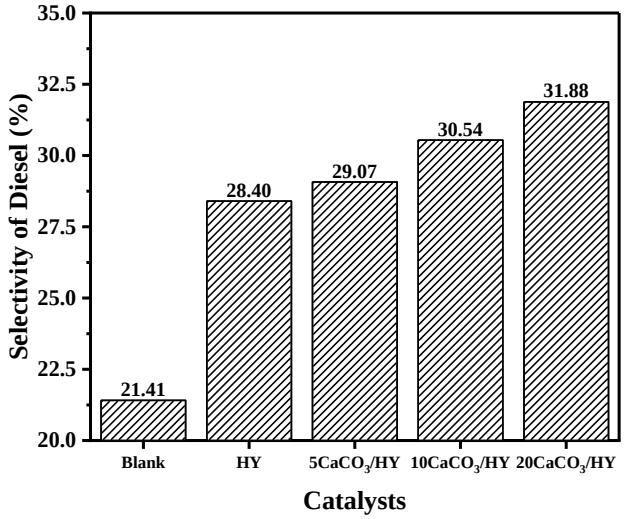

Figure 9. Effect of $CaCO_3$-modified catalysts on diesel range hydrocarbons product selectivity.

Table 7. Comparison of previous research on the cracking of palm oil into biofuel.

Catalyst	Temp. (°C)	Yield of OLP (%)	Selectivity (%)			Reference
			Gasoline	Kerosene	Diesel	
ZSM-5	450	68	69.77	9.51	5.04	(Riyanto *et al.*, 2021)
HZSM-5	450	65	45	17	3	(Bhatia *et al.*, 2009)
Ni/HY	410	46.3	69		19	(Li *et al.*, 2016)
HY	450	77.41	n.a.	n.a.	28.4	This study
$5CaCO_3$/HY	450	77.53	n.a.	n.a.	29.07	This study
$10CaCO_3$/HY	450	79.09	n.a.	n.a.	30.54	This study
$20CaCO_3$/HY	450	76.87	n.a.	n.a.	31.88	This study

*n.a : not available

The decreased catalyst surface area (compared to original HY catalyst) causes slight improvement of OLP or biofuel yield although the acidity strength of catalysts increased, while the increased catalyst average pore size leads to diesel hydrocarbon range selectivity. Because of the catalyst pore selectivity point of view, the $CaCO_3$/HY catalyst with high pore sizes may release the cracking product of long-chain hydrocarbons. Furthermore, the $CaCO_3$/HY catalyst has higher diesel selectivity than the HY catalyst due to pore size selectivity, as $CaCO_3$/HY has larger pore size than HY catalyst, and the pore structure may affect the catalyst activity in the cracking reaction (Li *et al.*, 2016). Li *et al.* (2021) also reported that the large pore size causes the liquid product to be quickly released from the surface. These findings may support improving catalyst stability of the $CaCO_3$/HY toward cracking deoxygenation of triglycerides due to its strong resistance to coke formation.

3.8. Proposed Reaction Mechanism of Catalytic Bifunctional Cracking-Deoxygenation using $CaCO_3$/HY Catalyst

Figure 10 illustrates a proposed reaction mechanism of catalytic bifunctional cracking-deoxygenation over $CaCO_3$/HY catalysts. In this reaction mechanism, the triglycerides are cracked through β-elimination and formed into a long-chain fatty acid. The C–C carbon chains of long-chain fatty acids are cracked through catalytic cracking reactions due to the roles of the high acid strength of acid sites (Brønsted and Lewis). As a result of the breakage of the double bonds in unsaturated acids, smaller chains of the hydrocarbon product are formed.

DOI: https://doi.org/10.17509/ijost.v8i2.55494
p- ISSN 2528-1410 e- ISSN 2527-8045

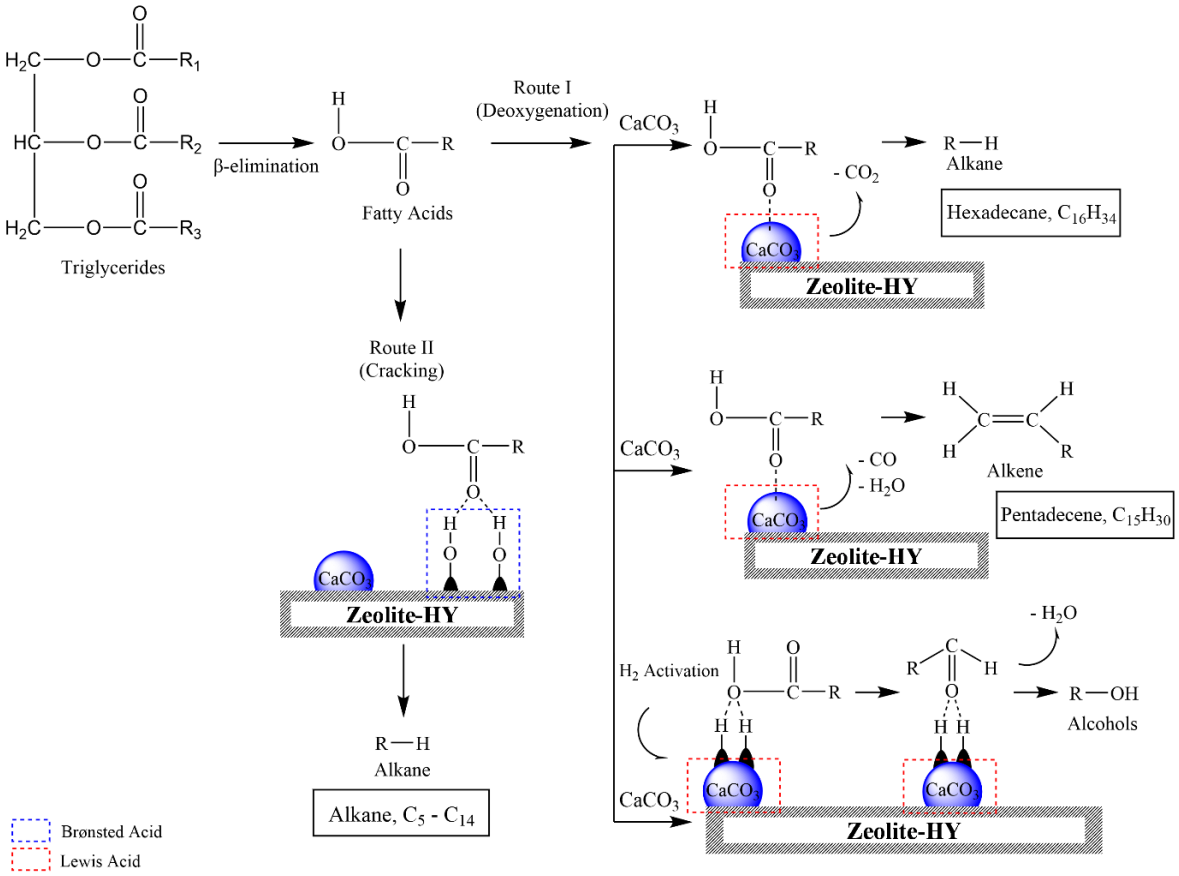

Figure 10. Proposed reaction mechanisms of catalytic cracking-deoxygenation over $CaCO_3$/HY catalysts.

Concerning deoxygenation reaction pathways, Srihanun *et al*. (2020) also reported that the deoxygenation process produces carbon dioxide (CO_2), carbon monoxide (CO), and water (H_2O) as byproducts. In the case of continuing cracking of the fatty acids after β-elimination, the deoxygenation reaction mechanism forms hydrocarbon chains containing C_{16}-C_{18} carbon atoms, while the hydrocarbon chains below C_{15} are formed by the cracking (β-scission) reactions (Istadi *et al.*, 2021b). Gosselink *et al.* (2013) also explained that decreased C_{17} chain length and increased short hydrocarbon chains (C_1–C_5) lead to stronger cracking activity due to the high strength of acidity catalyst properties, which is also confirmed in this study.

The main components of palm oil raw material are palmitic acid (C16:0) and oleic acid (C18:1) (**Table 1**), so it is possible to produce C_{15} and C_{17} hydrocarbons through cracking, decarboxylation, decarbonylation, and/or hydrodeoxygenation reaction pathways. Furthermore, the long fatty acids, as intermediates after β-elimination of triglyceride, are cracked via β-scission, as well as decarboxylation, decarbonylation, and/or hydrodeoxygenation reaction to form shorter chain hydrocarbons with lower oxygen content. Moreover, the C□O hydrogenolytic cleavage of the triglyceride molecule can also occur (Istadi *et al.*, 2021b). According to these findings, a strong acid base also plays important role in controlling the reactivity of the deoxygenation reaction. The $CaCO_3$-modified HY with high strong acid sites may convert the carboxylic acid groups to aldehydes and H_2O by chemisorption of the oxygen, bound in the carboxylic acid, on the catalyst surface.

3.9. Catalyst Stability Test

Catalyst stability is a critical issue in the palm oil cracking process, especially in the

DOI: https://doi.org/10.17509/ijost.v8i2.55494
p- ISSN 2528-1410 e- ISSN 2527-8045

continuous catalytic cracking process. In this study, the stability test was conducted to investigate the stability performance of 20$CaCO_3$/HY catalyst to convert palm oil to biofuel as a function of time on stream (TOS). The analysis was conducted for 23 h at 450 °C and WHSV of 0.288 min^{-1}. The yield of OLP and the selectivity of diesel fraction were monitored every 2 h of the continuous cracking process. The profiles of the yield of OLP and the selectivity of diesel are presented in **Figure 11**. The 20$CaCO_3$/HY catalyst showed good catalyst stability. The profile of the yield of OLP seems to be constant over the TOS of 23 h. In addition, the catalyst has also good stability for diesel production. As can be observed, the selectivity of diesel fraction decreases in a neglectable value over 23 h. Therefore, it can be concluded that the 20$CaCO_3$/HY catalyst has good stability for the palm oil cracking process to produce biofuel, especially in the diesel range.

4. CONCLUSION

Therefore, the designed catalysts ($CaCO_3$-modified HY) have the bifunctional roles required in cracking-deoxygenation reaction mechanisms, including carbon dioxide (CO_2) removal through the decarboxylation reaction pathway, carbon monoxide (CO) removal through decarbonylation reaction pathway, and H_2O removal from hydrodeoxygenation reaction pathway. The significant activities of cracking and deoxygenation (decarboxylation, decarbonylation, and hydrodeoxygenation) were enhanced by the high strength of acidity (due to Lewis and Brønsted acid site roles of a combination of $CaCO_3$ and HY) and basicity (due to $CaCO_3$ role) affected on the catalyst. In the proposed reaction mechanism, the triglycerides are cracked through β-elimination forming long-chain fatty acid. The C–C carbon chains of long-chain fatty acids are cracked through catalytic cracking reactions due to the roles of the high acid strength of acid sites (Brønsted and Lewis). Furthermore, the long fatty acids, as intermediates after β-elimination of triglyceride, are cracked via β-scission, as well as decarboxylation, decarbonylation, and/or hydrodeoxygenation reaction to form shorter chain hydrocarbons with lower oxygen content.

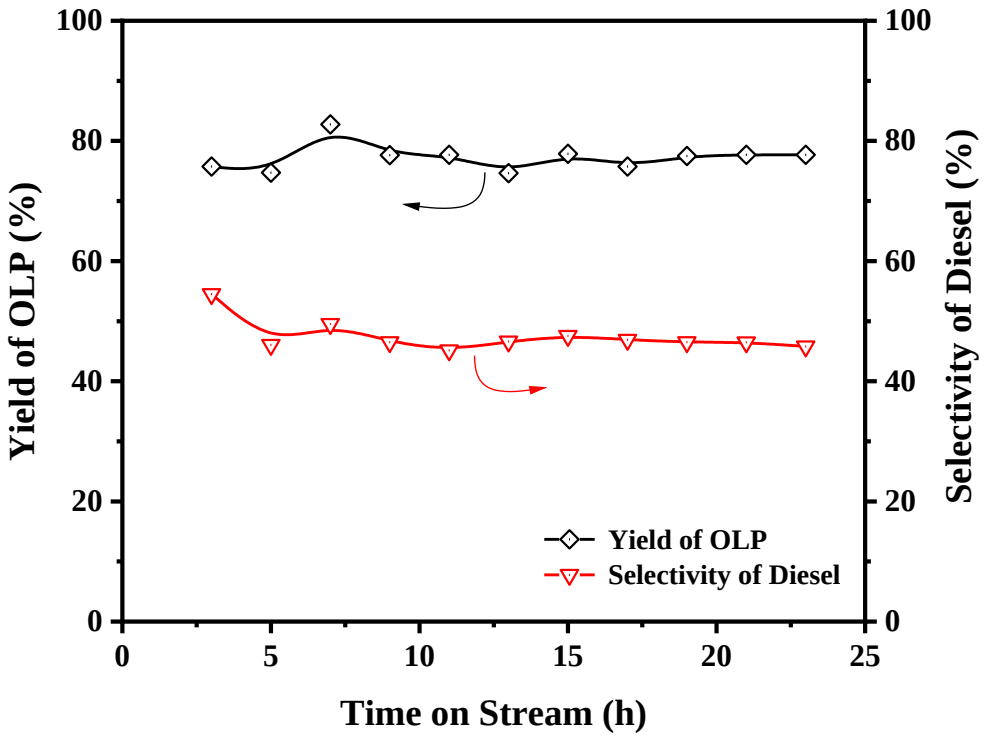

Figure 11. Stability test result of 20$CaCO_3$/HY catalyst for palm oil cracking process.

DOI: https://doi.org/10.17509/ijost.v8i2.55494
p- ISSN 2528-1410 e- ISSN 2527-8045

5. ACKNOWLEDGMENT

The authors would like to express their sincere gratitude to Research Institution and Community Service, Universitas Diponegoro, Indonesia, for the financial support through the World Class Research Universitas Diponegoro (WCRU) research project category A with contract number: 118-22/UN7.6.1/PP/2021.

6. AUTHORS' NOTE

The author(s) declare(s) that there is no conflict of interest regarding the publication of this article. The authors confirmed that the data and the paper are free of plagiarism.

7. REFERENCES

Al-Othman, Z. A. (2012). A Review: Fundamental aspects of silicate mesoporous materials. *Materials*, *5*(12), 2874–2902.

Anggoro, D. D., Buchori, L., Silaen, G. C. and Utami, R. N. (2017). Preparation, characterization, and activation of Co-Mo/Y zeolite catalyst for coal tar conversion to liquid fuel. *Bulletin of Chemical Reaction Engineering and Catalysis*, *12*(2), 219.

Asikin-Mijan, N., Lee, H. V., Juan, J. C., Noorsaadah, A. R. and Taufiq-Yap, Y. H. (2017). Catalytic deoxygenation of triglycerides to green diesel over modified CaO-based catalysts. *RSC Advances*, *7*(73), 46445–46460.

Asikin-Mijan, N., Lee, H. V., Juan, J. C., Noorsaadah, A. R., Abdulkareem-Alsultan, G., Arumugam, M. and Taufiq-Yap, Y. H. (2016). Waste clamshell-derived CaO supported Co and W catalysts for renewable fuels production via cracking-deoxygenation of triolein. *Journal of Analytical and Applied Pyrolysis*, *120*, 110–120.

Asikin-Mijan, N., Rosman, N. A., AbdulKareem-Alsultan, G., Mastuli, M. S., Lee, H. V., Nabihah-Fauzi, N., Lokman, I. M., Alharthi, F. A., Alghamdi, A. A., Aisyahi, A. A. and Taufiq-Yap, Y. H. (2020). Production of renewable diesel from jatropha curcas oil via pyrolytic-deoxygenation over various multi-wall carbon nanotube-based catalysts. *Process Safety and Environmental Protection*, *142*, 336–349.

Bhatia, S., Mohamed, A. R. and Shah, N. A. A. (2009). Composites as cracking catalysts in the production of biofuel from palm oil: Deactivation studies. *Chemical Engineering Journal*, 155 (1–2), 347–354.

Bonenfant, D., Kharoune, M., Niquette, P., Mimeault, M. and Hausler, R. (2008). Advances in principal factors influencing carbon dioxide adsorption on zeolites. *Science and Technology of Advanced Materials*, *9*(1), 13007.

Charisiou, N. D., Siakavelas, G., Tzounis, L., Sebastian, V., Monzon, A., Baker, M. A., Hinder, S. J., Polychronopoulou, K., Yentekakis, I. V. and Goula, M. A. (2018). An in depth investigation of deactivation through carbon formation during the biogas dry reforming reaction for Ni supported on modified with {CeO}2 and La2O3 zirconia catalysts. *International Journal of Hydrogen Energy*, *43*(41), 18955–18976.

Cheng, H., Zhang, J., Chen, Y., Zhang, W., Ji, R., Song, Y., Li, W., Bian, Y., Jiang, X., Xue, J. and Han, J. (2022). Hierarchical porous biochars with controlled pore structures derived from co-pyrolysis of potassium/calcium carbonate with cotton straw for efficient sorption of diethyl phthalate from aqueous solution. *Bioresource Technol*ogy, *346*, 126604.

DOI: https://doi.org/10.17509/ijost.v8i2.55494
p- ISSN 2528-1410 e- ISSN 2527-8045

Cheng, S., Wei, L., Julson, J., Muthukumarappan, K. and Kharel, P. R. (2017). Upgrading pyrolysis bio-oil to hydrocarbon enriched biofuel over bifunctional Fe-Ni/HZSM-5 catalyst in supercritical methanol. *Fuel Processing Technology*, *167*, 117–126.

Choo, M.-Y., Oi, L. E., Ling, T. C., Ng, E.-P., Lin, Y.-C., Centi, G. and Juan, J. C. (2020). Deoxygenation of triolein to green diesel in the H2-free condition: Effect of transition metal oxide supported on zeolite Y. *Journal of Analytical and Applied Pyrolysis*, *147*, 104797.

Corma, A. and Orchillés, A. V. (2000). Current views on the mechanism of catalytic cracking. *Microporous and Mesoporous Materials*, *35–36*, 21–30.

Dias, J. A. C. and Assaf, J. M. (2003). Influence of calcium content in Ni/CaO/γ-Al2O3 catalysts for CO2-reforming of methane. *Catalysis Today*, *85*(1), 59–68.

Doyle, A. M., Albayati, T. M., Abbas, A. S. and Alismaeel, Z. T. (2016). Biodiesel production by esterification of oleic acid over zeolite y prepared from kaolin. *Renew Energy*, *97*, 19–23.

Elias, S., Rabiu, A. M., Okeleye, B. I., Okudoh, V. and Oyekola, O. (2020). Bifunctional heterogeneous catalyst for biodiesel production from waste vegetable oil. *Applied Sciences*, *10*(9), 3153.

Ezeh, C. I., Yang, X., He, J., Snape, C. and Cheng, X. M. (2018). Correlating ultrasonic impulse and addition of ZnO promoter with CO2 conversion and methanol selectivity of CuO/ZrO2 catalysts. *Ultrasonics Sonochemistry*, *42*, 48–56.

Fathi, S., Sohrabi, M. and Falamaki, C. (2014). Improvement of HZSM-5 performance by alkaline treatments: Comparative catalytic study in the MTG reactions. *Fuel*, *116*, 529–537.

Gallei, E. and Stumpf, G. (1976). Infrared Spectroscopic studies of the adsorption of carbon dioxide and the coadsorption of carbon dioxide and water on CaY- and NiY-Zeolites. *Journal of Colloid and Interface Science*, *55*(2), 415–420.

Golubev, I. S., Dik, P. P., Kazakov, M. O., Pereyma, V. Yu., Klimov, O. V., Smirnova, M. Yu., Prosvirin, I. P., Gerasimov, E. Yu., Kondrashev, D. O., Golovachev, V. A., Vedernikov, O. S., Kleimenov, A. V. and Noskov, A. S. (2021). The effect of Si/Al ratio of zeolite Y in NiW catalyst for second stage hydrocracking. *Catalysis Today*, *378*, 65–74.

Gosselink, R. W., Hollak, S. A. W., Chang, S.-W., van Haveren, J., de Jong, K. P., Bitter, J. H. and van Es, D. S. (2013). Reaction pathways for the deoxygenation of vegetable oils and related model compounds. *ChemSusChem*, *6*(9), 1576–1594.

Hancsók, J., Magyar, S., and Holló, A. (2007). Importance of isoparaffins in the crude oil refining industry. *Chemical Engineering Transactions, 11*, 41–46.

Hartanto, D., Sin Yuan, L., Mutia Sari, S., Sugiarso, D., Kris Murwarni, I., Ersam, T., Prasetyoko, D. and Nur, H. (2016). The use of the combination of ftir, pyridine adsorption, 27Al and 29Si MAS NMR to determine the brönsted and lewis acidic sites. *Jurnal Teknologi*, *78*(6), 223–228.

Hermida, L., Abdullah, A. Z. and Mohamed, A. R. (2015). Deoxygenation of fatty acid to produce diesel-like hydrocarbons: A review of process conditions, reaction kinetics and mechanism. *Renewable and Sustainable Energy Reviews*, *42*, 1223–1233.

DOI: https://doi.org/10.17509/ijost.v8i2.55494
p- ISSN 2528-1410 e- ISSN 2527-8045

Huang, Y. C., Fowkes, F. M., Lloyd, T. B. and Sanders, N. D. (1991). Adsorption of calcium ions from calcium chloride solutions onto calcium carbonate particles. *Langmuir*, *7*(8), 1742–1748.

Huang, Z., Zhang, J., Li, P., Xu, L., Zhang, X., Yuan, Y. and Xu, L. (2017). Tert-butylation of naphthalene by tertiary butanol over HY zeolite and cerium-modified HY catalysts. *Catalysis Science & Technology*, *7*(20), 4700–4709.

Istadi, I., Riyanto, T., Buchori, L., Anggoro, D. D., Gilbert, G., Meiranti, K. A., and Khofiyanida, E. (2020a). Enhancing brønsted and lewis acid sites of the utilized spent rfcc catalyst waste for the continuous cracking process of palm oil to biofuels. *Industrial and Engineering Chemistry Research, 59*(20), 9459–9468.

Istadi, I., Riyanto, T., Buchori, L., Anggoro, D. D., Pakpahan, A. W. S. and Pakpahan, A. J. (2021a). Biofuels production from catalytic cracking of palm oil using modified HY zeolite catalysts over a continuous fixed bed catalytic reactor. *International Journal of Renewable Energy Development*, *10*(1), 149–156.

Istadi, I., Riyanto, T., Buchori, L., Anggoro, D. D., Saputra, R. A., Muhamad, T. G. (2020b). Effect of temperature on plasma-assisted catalytic cracking of palm oil into biofuels. *International Journal of Renewable Energy Development*, *9*(1), 107–112.

Istadi, I., Riyanto, T., Khofiyanida, E., Buchori, L., Anggoro, D. D., Sumantri, I., Putro, B. H. S. and Firnanda, A. S. (2021b). Low-oxygenated biofuels production from palm oil through hydrocracking process using the enhanced spent RFCC catalysts. *Bioresource Technology Reports*, *14*, 100677.

Jun, Y., Lee, S., Lee, K. and Choi, M. (2017). Effects of secondary mesoporosity and zeolite crystallinity on catalyst deactivation of ZSM-5 in Propanal conversion. *Microporous and Mesoporous Materials*, *245*, 16–23.

Khan, S., Kay Lup, A. N., Qureshi, K. M., Abnisa, F., Wan Daud, W. M. A. and Patah, M. F. A. A (2019). Review on deoxygenation of triglycerides for jet fuel range hydrocarbons. *Journal of Analytical and Applied Pyrolysis*, *140*, 1–24.

Kianfar, E., Salimi, M., Pirouzfar, V. and Koohestani, B. (2018). Synthesis and modification of zeolite ZSM-5 catalyst with solutions of calcium carbonate (CaCO3) and sodium carbonate (Na2CO3) for methanol to gasoline conversion. *International Journal of Chemical Reactor Engineering*, *16*(7), 1-7.

Kubička, D., Horáček, J., Setnička, M., Bulánek, R., Zukal, A. and Kubičková, I. (2014). Effect of support-active phase interactions on the catalyst activity and selectivity in deoxygenation of triglycerides. *Applied Catalysis B: Environmental*, *145*, 101–107.

Kwon, K. C., Mayfield, H., Marolla, T., Nichols, B., and Mashburn, M. (2011). Catalytic deoxygenation of liquid biomass for hydrocarbon fuels. *Renew Energy*, *36*(3), 907–915.

Lawan, I., Garba, Z. N., Zhou, W., Zhang, M. and Yuan, Z. (2020). Synergies between the Microwave Reactor and CaO/zeolite catalyst in waste lard biodiesel production. *Renew Energy*, *145*, 2550–2560.

Li, S.-C., Lin, Y.-C. and Li, Y.-P. (2021). Understanding the catalytic activity of microporous and mesoporous zeolites in cracking by experiments and simulations. *Catalysts*, *11*(9), 1114.

DOI: https://doi.org/10.17509/ijost.v8i2.55494
p- ISSN 2528-1410 e- ISSN 2527-8045

Li, T., Cheng, J., Huang, R., Yang, W., Zhou, J. and Cen, K. (2016). Hydrocracking of palm oil to jet biofuel over different zeolites. *International Journal of Hydrogen Energy*, *41*(47), 21883–21887.

Liu, L. and Corma, A. (2018). Metal catalysts for heterogeneous catalysis: From single atoms to nanoclusters and nanoparticles. *Chemical Reviews*, *118*(10), 4981–5079.

Meng, B., Ren, S., Zhang, X., Chen, K., Wei, W., Guo, Q. and Shen, B. (2022). Enhancement of the strong brønsted acidity and mesoporosity: Zr4+ promoted framework modification of zeolite Y. *Microporous and Mesoporous Materials*, *335*, 111849.

Munnik, P., de Jongh, P. E. and de Jong, K. P. (2015). Recent developments in the synthesis of supported catalysts. *Chemical Reviews*, *115*(14), 6687–6718.

Oenema, J., Hofmann, J. P., Hensen, E. J. M., Zečević, J. and Jong, K. P. (2020). Assessment of the location of Pt nanoparticles in Pt/Zeolite Y/Γ-Al2O3 composite catalysts. *ChemCatChem*, *12*(2), 615–622.

Ooi, X. Y., Gao, W., Ong, H. C., Lee, H. V., Juan, J. C., Chen, W. H. and Lee, K. T. (2019). Overview on catalytic deoxygenation for biofuel synthesis using metal oxide supported catalysts. *Renewable and Sustainable Energy Reviews*, *112*, 834–852.

Oyebanji, J. A., Okekunle, P. O. and Fayomi, O. S. I. (2020). Synthesis and characterization of zeolite-Y using ficus exasperata leaf: A preliminary study. *Case Studies in Chemical and Environmental Engineering*, *2*, 100063.

Papageridis, K. N., Charisiou, N. D., Douvartzides, S., Sebastian, V., Hinder, S. J., Baker, M. A., AlKhoori, S., Polychronopoulou, K. and Goula, M. A. (2020). Promoting effect of CaO-MgO mixed oxide on Ni/γ-Al2O3 catalyst for selective catalytic deoxygenation of palm oil. *Renew Energy*, *162*, 1793–1810.

Peng, X., Cheng, K., Kang, J., Gu, B., Yu, X., Zhang, Q. and Wang, Y. (2015). Impact of hydrogenolysis on the selectivity of the fischer-tropsch synthesis: Diesel fuel production over mesoporous zeolite-Y-supported cobalt nanoparticles. *Angewandte Chemie*, *127*(15), 4636–4639.

Phung, T. K., Casazza, A. A., Aliakbarian, B., Finocchio, E., Perego, P. and Busca, G. (2013). Catalytic conversion of ethyl acetate and acetic acid on alumina as models of vegetable oils conversion to biofuels. *Chemical Engineering Journal*, *215–216*, 838–848.

Puriwat, J., Chaitree, W., Suriye, K., Dokjampa, S., Praserthdam, P. and Panpranot, J. (2010). Elucidation of the basicity dependence of 1-butene isomerization on MgO/Mg(OH)2 catalysts. *Catalysis Communication*, *12*(2), 80–85.

Putluru, S. S. R., Jensen, A. D., Riisager, A. and Fehrmann, R. (2011). Alkali resistant fe-zeolite catalysts for SCR of NO with NH3 in flue gases. *Topics in Catalysis*, *54* (16–18), 1286–1292.

Ramesh, A., Tamizhdurai, P. and Shanthi, K. (2019). Catalytic hydrodeoxygenation of jojoba oil to the green-fuel application on NI-MoS/Mesoporous Zirconia-Silica Catalysts. *Renew Energy*, *138*, 161–173.

Riyanto, T., Istadi, I., Buchori, L., Anggoro, D. D., and Dani Nandiyanto, A. B. (2020). Plasma-assisted catalytic cracking as an advanced process for vegetable oils conversion to

DOI: https://doi.org/10.17509/ijost.v8i2.55494
p- ISSN 2528-1410 e- ISSN 2527-8045

biofuels: A mini review. *Industrial and Engineering Chemistry Research*, *59*(40), 17632–17652.

Riyanto, T., Istadi, I., Jongsomjit, B., Anggoro, D. D., Pratama, A. A. and al Faris, M. A. (2021). Improved brønsted to lewis (B/L) ratio of Co- and Mo-impregnated ZSM-5 catalysts for palm oil conversion to hydrocarbon-rich biofuels. *Catalysts*, *11*(11), 1286.

Santillan-Jimenez, E. and Crocker, M. (2012). Catalytic deoxygenation of fatty acids and their derivatives to hydrocarbon fuels via decarboxylation/decarbonylation. *Journal of Chemical Technology and Biotechnology*, *87*(8), 1041–1050.

Sartipi, S., Makkee, M., Kapteijn, F. and Gascon, J. (2014). Catalysis engineering of bifunctional solids for the one-step synthesis of liquid fuels from syngas: A Review. *Catalysis Science & Technology*, *4*(4), 893–907.

Seifi, H. and Sadrameli, S. M. (2016). Improvement of renewable transportation fuel properties by deoxygenation process using thermal and catalytic cracking of triglycerides and their methyl esters. *Applied Thermal Engineering*, *100*, 1102–1110.

Shakirova, L. Kh., Pluzhnikova, M. F. and Tsybulevskii, A. M. (1980). Mechanism of catalytic cracking of hydrocarbons on zeolites. *Petroleum Chemistry U.S.S.R.*, *20*(1), 45–54.

Srihanun, N., Dujjanutat, P., Muanruksa, P. and Kaewkannetra, P. (2020). Biofuels of green diesel–kerosene–gasoline production from palm oil: Effect of palladium cooperated with second metal on hydrocracking reaction. *Catalysts*, *10*(2), 241.

Suárez, N., Pérez-Pariente, J., Márquez-Álvarez, C., Grande Casas, M., Mayoral, A. and Moreno, A. (2019). Preparation of mesoporous beta zeolite by fluoride treatment in liquid phase. textural, acid and catalytic properties. *Microporous and Mesoporous Materials*, *284*, 296–303.

Sugiyama, S., Sakuwa, Y., Ogino, T., Sakamoto, N., Shimoda, N., Katoh, M. and Kimura, N. (2019). Gas-phase epoxidation of propylene to propylene oxide on a supported catalyst modified with various dopants. *Catalysts*, 9, 638.

Suprun, W., Lutecki, M., Haber, T. and Papp, H. (2009). Acidic catalysts for the dehydration of glycerol: Activity and deactivation. *Journal of Molecular Catalysis A: Chemical*, *309* (1–2), 71–78.

Tsai, W.-T. (2013). Microstructural characterization of calcite-based powder materials prepared by planetary ball milling. *Materials*, *6*(8), 3361–3372.

Twaiq, F. A. A., Mohamad, A. R. and Bhatia, S. (2004). Performance of composite catalysts in palm oil cracking for the production of liquid fuels and chemicals. *Fuel Processing Technology*, *85*(11), 1283–1300.

Wang, H., Lin, H., Zheng, Y., Ng, S., Brown, H., and Xia, Y. (2019). Kaolin-based catalyst as a triglyceride FCC upgrading catalyst with high deoxygenation, mild cracking, and low dehydrogenation performances. *Catalysis Today*, *319*, 164–171.

Wang, X., Fang, Q., Wang, J., Gui, K. and Thomas, H. R. (2020). Effect of CaCO3 on catalytic activity of Fe–Ce/Ti catalysts for NH3-SCR reaction. *RSC Adv*ances, *10*(73), 44876–44883.

DOI: https://doi.org/10.17509/ijost.v8i2.55494
p- ISSN 2528-1410 e- ISSN 2527-8045

Wei, T., Wang, M., Wei, W., Sun, Y. and Zhong, B. (2003). Effect of base strength and basicity on catalytic behavior of solid bases for synthesis of dimethyl carbonate from propylene carbonate and methanol. *Fuel Processing Technology*, *83*(1–3), 175–182.

Xu, Z.-X., Liu, P., Xu, G.-S., Liu, Q., He, Z.-X., and Wang, Q. (2017). Bio-fuel oil characteristic from catalytic cracking of hydrogenated palm oil. *Energy*, *133*, 666–675.

Yi, L., Liu, H., Xiao, K., Wang, G., Zhang, Q., Hu, H. and Yao, H. (2019). In Situ upgrading of bio-oil via CaO catalyst derived from organic precursors. *Proceedings of the Combustion Institute*, *37*(3), 3119–3126.

Yigezu, Z. D. and Muthukumar, K. (2014). Catalytic cracking of vegetable oil with metal oxides for biofuel production. *Energy Conversion and Management*, *84*, 326–333.

Zhao, W., Huang, J., Ni, K., Zhang, X., Lai, Z., Cai, Y. and Li, X. (2018). Research on non-thermal plasma assisted HZSM-5 online catalytic upgrading bio-oil. *Journal of the Energy Institute*, *91*(4), 595–604.

Zhao, X., Wei, L., Cheng, S. and Julson, J. (2015). Optimization of catalytic cracking process for upgrading camelina oil to hydrocarbon biofuel. *Industrial Crops and Products*, *77*, 516–526.

Zhao, X., Wei, L., Julson, J., Gu, Z. and Cao, Y. (2015). Catalytic cracking of inedible camelina oils to hydrocarbon fuels over bifunctional Zn/ZSM-5 catalysts. *Korean Journal of Chemical Engineering*, *32*(8), 1528–1541.

Zheng, Y., Guo, Y., Wang, J., Luo, L. and Zhu, T. (2021). Ca doping effect on the competition of NH3–SCR and NH3 oxidation reactions over vanadium-based catalysts. *The Journal of Physical Chemistry C*, *125*(11), 6128–6136.

DOI: https://doi.org/10.17509/ijost.v8i2.55494
p- ISSN 2528-1410 e- ISSN 2527-8045